Fluid Mechanics of the Planar-Flow Melt-Spinning Process

The planar-flow melt-spinning process which is used to rapidly solidify metals from the molten state is shown to be dominated by the fluid mechanics of the "puddle" region even though heat-transfer limits the overall thickness of the metal ribbon product. The process is modeled to account for the hydrodynamical forces in the molten region with the influence of heat-transfer entering through a parameter measuring solidification rate relative to wheel speed. It is shown that this parameter H controls the deviation of the flow behavior from classical coating flow solutions; these solutions are recovered in a limiting case of low solidification rate. A perturbation solution in H distinguishes the melt spinning from the coating process and yields the ribbon thickness as a function of wheel-speed and the other process parameters for a class of contact-line conditions. Most interesting of these predictions is the result that under certain conditions there is a window of wheel-speeds for which there is no steady solution. The relationship of predictions with the limited available data from experiment is briefly discussed.

Paul H. Steen and J. Kent Carpenter
School of Chemical Engineering
Cornell University
Ithaca, NY 14853

Ho Yu
Alcoa Technical Center
Alcoa Center, PA 15069

Introduction

Metals which are rapidly solidified from the molten state are known to exhibit electrical, chemical and mechanical properties that are quite different from their slowly cooled counterparts. Commercial products based on these special properties include superalloy materials (high-temperature strength and forgeability) used in high-performance gas turbine engines (Miller, 1986), electrical core materials (high electrical resistance) used in transformers and electric motors (Belden, 1985), and magnetic materials (both hard and soft) for devices requiring high-performance reasonably-priced magnets (Koon, 1986). The melt-spinning technique of rapid solidification, Figure 1, achieves relatively high cooling rates (10^6 K/s) and offers the economic advantages of a continuous process.

The planar-flow version of melt spinning is a configuration in which the nozzle that directs the molten metal onto the rapidly rotating chilled wheel is brought so close to the wheel that the nozzle lip itself restricts the flow, Figure 1a. This geometrical arrangement generates a "puddle" of molten metal beneath the rectangular lip of the nozzle; the gap between wheel and nozzle forms a nearly parallel-walled planar channel with the wheel-side moving rapidly. The solidified metal is spun off as a thin ribbon; a typical velocity is 10 m/s.

Planar-flow melt spinning (Narasimhan, 1979) was developed in the early to mid-1970s to increase the cast width of ribbon over that attainable when the nozzle is placed at some distance from the chill wheel, so-called "chill-block" melt spinning, Figure 1b (Guntherodt, 1985). Among the early studies of the "chill-block" process, the noteworthy work of Kavesh (1978) distinguishes thermal- and momentum-transport-limited cases, a distinction which we shall redraw below in the context of the planar-flow process. In the chill-block process, where the primary control parameters are the flow rate of molten metal and the wheel-speed, the balance of mass shows that the thickness of the ribbon is inversely proportional to the wheel-speed provided the width of the ribbon is constant. The inertia of the molten metal stream as altered by the wheel is balanced by the melt surface tension to form a puddle which controls the ribbon width. A wide range of experiments shows that the width varies significantly with wheel-speed and consequently thickness varies to some inverse power of speed which deviates from unity (e.g., Hillmann and Hilzinger, 1978). In contrast, the primary

Correspondence concerning this paper should be addressed to P. H. Steen.

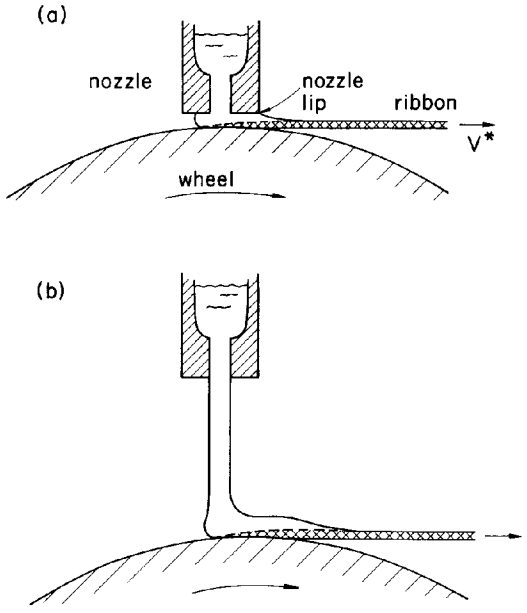

Figure 1. Melt-spinning process: a) planar-flow; b) chill-block configuration.

control parameters of the planar-flow process are the pressure-drop imposed across the system (nozzle pressure relative to ambient) and the wheel speed which balance the combination of viscous force generated in the shear flow under the nozzle and the capillary force from the meniscus region with contributions (perhaps) from inertial forces. Although the width of the ribbon is fixed by the width of the nozzle slot, results from the analysis below show that the thickness is generally not inversely proportional to the substrate velocity. Indeed, parameters can be chosen so that thickness remains relatively unchanged or even increases with wheel speed although the latter behavior is expected to be unstable. Analyses of the chill-block process are apparently of limited relevance to the planar-flow technique.

Present-day commercial control of the process is largely based on experience or empirical knowledge. To attain the amorphous or microcrystalline microstructures which lead to special material properties rates of solidification must be sufficiently high. It is well-known that given a particular metal and its heat-transfer properties this implies an upper limit to the thickness of the ribbon (Jones, 1982). We argue below that within this limitation the primary influence of the heat-transfer is through the solidification rate.

We first develop a model for the solidification front based on the role of the heat-transfer and introduce the control parameter H which measures solidification rate relative to the wheel speed. Then the framework for the fluid mechanics is constructed by scaling the Navier-Stokes equations for flow fields linked to one another in series. These include the flow from the nozzle to the gap which forms a turning region, flow between the wheel and nozzle lip which has a nearly-rectilinear structure, and the flow downstream of the nozzle lip under the meniscus which is dominated by the surface tension. Classical coating flow solutions are then recovered in the limit of vanishing H. Small, but nonzero solidification rates are considered next and dependence of ribbon thickness on operating parameters is obtained. Finally, the relationship to results of experiment is discussed.

Solidification Front

The solidification front which stretches from the first point of contact of the molten metal with the chill-wheel downstream to the point where the last metal solidifies forms a curved interface under steady conditions. For purposes of predicting ribbon thicknesses and in the range of wheel-speeds of practical interest an average rate of solidification H^* (dimensional) can be used to characterize the heat transport.

This conclusion is reached by considering two limiting cases of solidification. In the first idealization, a continuous thin steady stream of molten metal strikes a good quenching agent which solidifies the stream into a wire at the position of first contact, Figure 2a. The small cross-section of the stream along with the effectiveness of the quencher imply that increases in flow rate will be matched by increases in solidification rate. Here, the speed of solidification is limited only by the flow rate, or in other words, by the flux of momentum into the quench-region.

In the second case, a planar solidification front propagating into the melt translates parallel to itself. If the rate of translation is much greater than the solidification rate, the dominant balance of heat transfer in a laboratory frame involves convection in the direction of translation, Figure 2b. Here, the solidification front is well approximated by an isotherm since latent heat generation is negligible relative to the contribution of convection. This is a high Peclet number situation.

In the planar flow process there exists some combination of these two limiting cases. In particular, near the upstream contact where the solidified layer is thinnest there must be a region, however narrow, of momentum-flux-limited solidification while downstream of that the heat transfer must be nearly indepen-

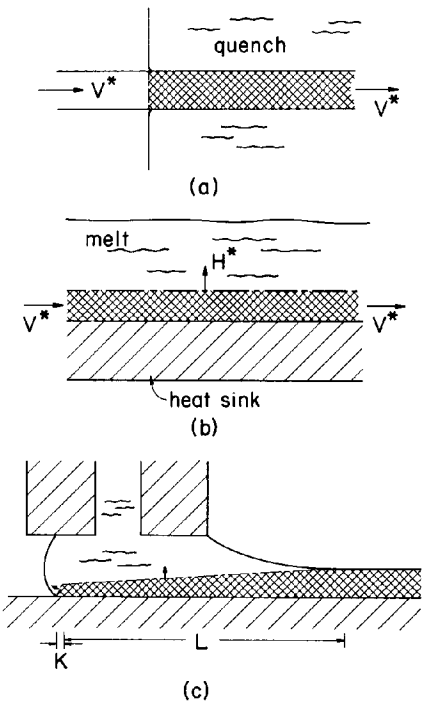

Figure 2. Solidification rate limited a) by flow rate of molten metal; b) by horizontal convection of heat; and c) by some combination of flow rate, K, and convection, L, in the planar flow process.

dent of the translation velocity. Figure 2c shows a schematic of the solidification front for the planar-flow process. If the flow-rate-limited region is negligibly small then the solidification rate can be approximated by a single speed, fixed for a particular molten material, constitution of chill-wheel, superheat temperature, and wheel temperature.

There is experimental evidence to justify this assumption. Chu, Giron, and Granger (1986) have placed a second nozzle a distance downstream of the first; this enables a second layer to be added on top of the initial thickness and by varying the downstream distance and by examining cross-sections of resultant microstructure they determine the horizontal extent of the molten region and thereby its average speed. They measure a value which indicates a nearly horizontal front corroborating the schematic of Figure 3. Furthermore, they find this rate H^* to be relatively insensitive to wheel speed, nozzle geometry and position, and pressure drop. This characterization of the influence of heat transfer on the process circumvents the modeling of a thermal field which must rely on estimates for the heat-transfer coefficient between the melt and wheel surface—a quantity recognized to be difficult to measure and to predict (Davies, 1985).

Fluid Mechanics

Miyazawa and Szekely (1979, 1981) seem to have first exploited the tremendous simplification implied by the lubrication nature of the related piston-and-anvil and twin-roll rapid-solidification techniques. Gutierrez (1985) carried this approximation over to an analysis of the planar-flow process. However, he imposed a fixed flow rate through the system which misrepresents actual operating conditions and so artificially constrains the problem. On the other hand, Yu (1987) imposes the overall pressure drop in an analysis which predicts ribbon thickness as a function of pressure drop, wheel speed, nozzle diameter and lubrication gap. He separates the planar-flow process into a nozzle flow, a lubrication flow between a stationary and moving plate, and lubrication flow between the moving plate and a shear-free meniscus accounting for the pressure drops across each leg of the process. Yu's limited experimental data show reasonably good agreement with the predictions of the model. A deficiency of his analysis, however, is that pressures within the puddle region are much larger than any static meniscus can sustain. A consistent formulation requires modification of Yu's ideas to account for the dominance of capillary forces in the meniscus region and leads to a closed form dependence of ribbon thickness on the operating parameters. Our framework for the fluid mechanics of the process is based on asymptotics suggested by three relevant dimensionless parameters. However, we leave for a later development perhaps the most noteworthy contribution of Yu's work, the suggestion based on preliminary evidence that surface irregularities in the ribbon derive from a meniscus instability.

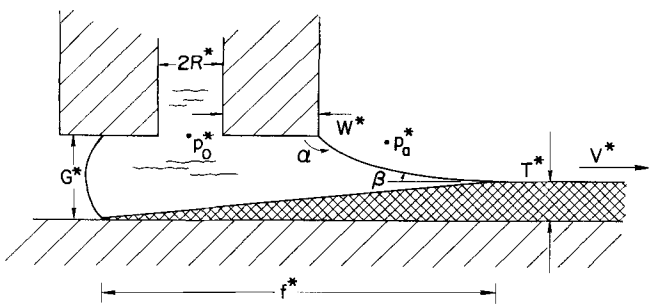

Figure 3. Definition of the dimensional variables.

A nozzle with a rectangular slot-like orifice (small dimension in flow direction) favors wider ribbons and is typical of planar-flow configurations. Provided the slot is narrow enough the flow in the nozzle does not vary in the cross-stream direction and is effectively two dimensional. The nearly rectangular platform of the puddle region indicates that slot extent fixes the ribbon width; the streamwise contact lines where the ribbon, wheel and ambient atmosphere meet are relatively stable.

The mass balance relates the ribbon thickness T^* to the streamwise extent of the liquid puddle f^* (the ribbon width is constant throughout the flow),

$$T^*V^* = H^*f^* \tag{1}$$

Here V^* is linear wheel speed and H^* is the solidification rate. The length f^* is an unknown function of wheel speed, pressure drop, geometry and material properties. The object of study is the function f^* and we note that if f^* depends only weakly on its arguments then ribbon thickness will vary nearly inversely with wheel speed.

Dimensional analysis shows that even if the wheel/nozzle configuration is characterized by only three lengths, Figure 3 and Table 1, the function f^* will depend on six nondimensional groups. Here and in what follows we make the nonessential assumption $\rho_s = \rho_l$ for simplicity. In dimensionless form, $f \equiv f^*/G^*$, and using the definitions of Table 1,

$$T/H = f\{Re, Ca, H, \Delta p, R, W\} \tag{2}$$

The model outlined below obtains the functional dependence of f on its arguments. Although characteristic temperature gradients for the system are on the order of 10^4 K/m, the dimensional analysis and the analyses to follow take material properties to be constant since such variations are not at the heart of the physics.

Table 1. Typical Values for the Physical and Process Parameters and for the Dimensionless Groups

Nozzle Geometry	
$G^* = 5 \times 10^{-4}$m	Nozzle/wheel gap
$R^* = 4 \times 10^{-4}$ m	Nozzle slot width
$W^* = 10^{-2}$ m	Nozzle lip extent
Process Variables	
$T^* = 10^{-4}$ m	Ribbon thickness
$H^* = 2 \times 10^{-1}$ m/s	Solidification rate
$V^* = 10$ m/s	Linear wheel speed
$P_o^* - P_a^* = 3 \times 10^3$ N/m^2	Pressure drop
Material Properties (Aluminum)	
$\rho_s = 2.7 \times 10^3$ kg/m^3	Solid density
$\rho_e = 2.3 \times 10^3$ kg/m^3	Molten density (1,033 K)
$\mu = 10^{-3}$ kg/m · s	Viscosity (1,033 K)
$\sigma = 1$ N/m	Surface tension (1,033 K)
Derived Dimensionless Groups	
$Re = 2{,}300$	Reynolds number
$W = 0.4$	
$H = 2 \times 10^{-2}$	Slope of converging geometry
$Ca = 5 \times 10^{-3}$	Capillary number
$R = 0.8$	
$\Delta p = 0.1$	

The hydrodynamic behavior of the planar-flow process is split into three regions connected in series: (i) the flow which turns from the nozzle exit into the gap; (ii) the flow in the gap extending to the start of the meniscus; and (iii) the flow between the free meniscus and the solidified substrate extending downstream until solidification is complete, Figure 4. The meniscus can detach before the front edge of the nozzle lip in which case a fixed contact angle may be assumed or it can detach at the sharp lip edge in which case a fixed contact line is appropriate. Results will be reported for both boundary conditions. The flow upstream of region (i) may also contribute to the pressure applied in any experiment. However, typically this flow is easy to characterize (e.g., a Poiseuille flow) and hence its effect on the predictions presented below can be readily accounted for.

Turning flow

Region (i) will be denoted Ω. The flow entering the region is assumed to be fully developed and to be steady. The Reynolds number Re = 2,300 based on mass flow, Table 1, is well below the critical value for instability of plane Poiseuille flow [Re_c = 7,696, same basis (Orszag, 1971)], although the latter value may be only of limited relevance since disturbances in a typical process will have finite amplitudes. The "engineering" stability limit is Re_c = 2,800 (Hanks and Rao, 1966) which suggests that practical operating regimes not considered here may involve turbulent flow. The entrance to (AB) and the exit from (CD) region (i) are chosen sufficiently far upstream and downstream, respectively, that the velocities v^* have no transverse components and that the pressures p^* are uniform across these sections. An account of the rate of change of mechanical energy within the region gives a balance between the rate of work done on the boundary of Ω by the pressures at the entrance and exit and by the shear stress τ^* at the moving wall, the flux of kinetic energy through the boundary, and the dissipation within the region, all taken per unit volume,

$$p_0^* - p_1^* = \frac{1}{2}\rho(\gamma_1\langle v^*\rangle_{CD}^2 - \gamma_0\langle v^*\rangle_{AB}^2) - \langle\tau^*\rangle_{ED}V^*x_1^*/\langle v^*\rangle_{CD}G^* + \int_\Omega \Phi^*\,dv/\langle v^*\rangle_{CD}G^* \tag{3a}$$

where

$$\gamma_0 \equiv \langle v^{*3}\rangle_{AB}/\langle v^*\rangle_{AB}^3 \tag{3b}$$

$$\gamma_1 \equiv \langle v^{*3}\rangle_{CD}/\langle v^*\rangle_{CD}^3 \tag{3c}$$

and Φ^* is the pointwise viscous dissipation per unit volume, and the brackets denote averages over line segments of the boundary indicated by the subscripts. Here we have assumed

$$2R^*\langle v^*\rangle_{AB} \approx G^*\langle v^*\rangle_{CD}$$

which neglects the volume flux of solidified material at cross section CD, consistent with the assumption $x_2^* \gg x_1^*$.

If the rear meniscus were a static meniscus the maximum pressure sustainable would be $2\sigma/G^*$. This estimate for the pressure at "blowout" is used to scale the pressure drop in Eq. 3 which with the velocity scale V^* and length scale G^* leads to the following dimensionless version of Eq. 3:

$$p_0 - p_1 = (ReCa/T)\{\tfrac{1}{2}T^2[\gamma_1 - \gamma_0/4R^2] - g(Re, x_1) + h(Re, x_1)\} \tag{4a}$$

where

$$g \sim k_g x_1 Re^{-1} + O(Re^{-1/2}) \tag{4b}$$

$$h \sim k_h x_1 Re^{-1} + O(1) \tag{4c}$$

and k_g and k_h are constants in the asymptotic expansions of the work done by the plate g and of the dissipation losses h. If the pressure p_0 is large enough the fluid does work on the moving plate and expression 4b is inappropriate. However, such pressures always violate the blowout condition for the cases of interest in this paper (i.e., cases $H \to 0$). In all cases evaluated below the pressure drop across region (i) will be negligible relative to other pressure drops, a conclusion which depends on k_g and k_h being constants of order unity but which is independent of their particular values.

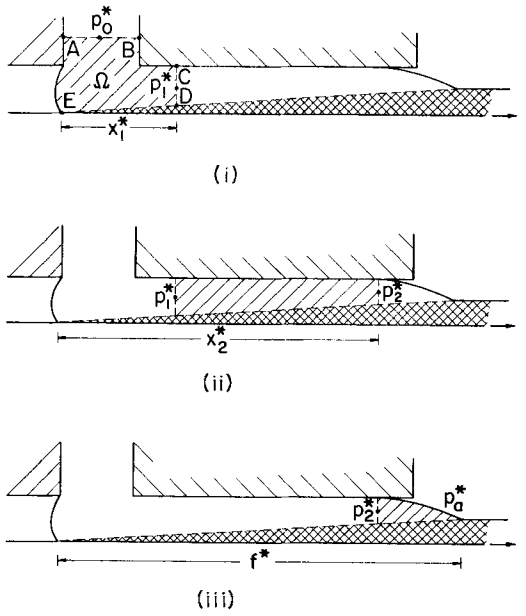

Figure 4. Three flow regimes: i) turning flow; ii) nearly-rectilinear flow; and iii) flow under the meniscus.

Nearly-rectilinear flow

The entrance to region (ii) is chosen so that the flow is well-developed there. The slightly inclined solidification front (slope H^*/V^*) forms a converging channel generating streamlines that are nearly parallel to the plate. The scaling appropriate for this nearly rectilinear flow is described by Ruschak (1985) and the resulting governing equations are

$$u_x + v_y = 0 \tag{5a}$$

$$(ReH/T)(uu_x + vu_y) = -p_x + u_{yy} + H^2u_{xx} \tag{5b}$$

$$(ReH^3/T)(uv_x + vv_y) = -p_y + H^2v_{yy} + H^4v_{xx} \tag{5c}$$

where the coordinates x and y are parallel and perpendicular to the plate with corresponding velocities u and v, respectively. The pressure is p and subscripts denote partial derivatives. The limiting case

$$ReH \to 0 \tag{5d}$$

$$H \to 0 \tag{5e}$$

leaves the equations that govern the classical lubrication layer. The lubrication equations are solved subject to boundary conditions of no slip at the top surface, no slip on the bottom solidified substrate, and detachment of the meniscus at the coordinate $x = x_2^*$. Rescaling the solution in order to employ the same scales as in system (Eq. 4) with the exception that the lubrication length x_2^* is scaled with W^*,

$$x_2^* = W^* x_2 \tag{6a}$$

and consistent with lubrication, defining W,

$$W \equiv HW^*/G^* \sim O(1) \text{ as } H \to 0 \tag{6b}$$

yields

$$p_1 - p_2 = \frac{6(Ca/H)(Wx_2 - Hx_1)}{(1 - Hx_1)^2(1 - Wx_2)^2} \cdot [T(2 - (Hx_1 + Wx_2)) - (1 - HWx_1x_2)] \tag{7}$$

The solution (Eq. 7) includes a pressure drop due to the frictional effects of the viscous fluid and a pressure rise due to work done by the moving wheel.

Meniscus Flow

Region (iii) begins at the meniscus detachment position x_2^* which is unknown *a priori* for the case of fixed contact angle or which is put equal to the lip length for the case of fixed contact line. The governing equations, scaled as in region (i), are written

$$u_x + v_y = 0 \tag{8a}$$

$$Re(Ca/T)(uu_x + vu_y) = -p_x + Ca(u_{xx} + u_{yy}) \tag{8b}$$

$$Re(Ca/T)(uv_x + vv_y) = -p_y + Ca(v_{xx} + v_{yy}) \tag{8c}$$

with normal stress and shear stress boundary conditions applied at the free interface,

$$p - p_a = -2\,Ca\frac{\partial u_n}{\partial n} - \kappa \tag{8d}$$

$$0 = \frac{\partial u_t}{\partial n} \tag{8e}$$

Here κ is the mean curvature, subscripts n and t denote the components normal and tangential to the interface respectively, and partial derivatives are in the direction normal to the interface.

The final boundary condition for system (Eqs. 8) involves the contact line on the moving substrate defined by the farthest point downstream where molten metal solidifies. Depending on the other parameters two physically distinct situations can occur at this downstream contact line. If all the molten metal which arrives there is solidified the fluid makes contact at a fixed angle which accommodates the difference between solid and liquid densities (angle zero for $\rho_s = \rho_l$) and there is no singularity. On the other hand, if some of the molten metal arriving there eventually returns upstream the contact line is a moving contact line with the associated singularity inherent in the physics due to a multiple-valued velocity field (Dussan V, 1979). In this case a constitutive relation between contact angle and velocity of the contact line is needed to complete the problem specification.

In the limiting case,

$$Ca \to 0 \tag{9a}$$

$$ReCa \to 0 \tag{9b}$$

the system (Eqs. 8) has the solution of a static fluid with uniform pressure dictating an interface shape of constant curvature. From elementary differential geometry the only surfaces with this characteristic are the circle and its limiting case the straight line. In terms of the dimensionless radius A of the circle,

$$p_2 - p_a = 1/A \tag{10}$$

The solution is completed by fitting a member of this family of interface shapes to the appropriate boundary conditions.

The pressure drops due to the flow fields (i), (ii), and (iii) are added to obtain the overall pressure drop and the resulting relationship is inverted for the ribbon thickness in order to obtain the function f, Eq. 2.

Coating Flow Limits

When capillary forces dominate the viscous forces in the three flow regions to the extent that

$$ReCa \to 0 \tag{11a}$$

$$Ca/H \to 0 \tag{11b}$$

$$ReH \to 0 \tag{11c}$$

as

$$Ca \to 0, \quad H \to 0 \tag{11d, e}$$

the flows are nearly static with uniform pressures and the net pressure drop across the system is due to the meniscus curvature. If we specify further,

$$\Delta p \equiv p_0 - p_a = 0 \tag{12}$$

then the meniscus curvature must vanish by Eq. 10. The limiting meniscus is a straight line. The coating flow limits are recovered for the class of boundary conditions for which the meniscus detaches at the nozzle lip-edge.

Requirement (11c) makes the limiting sequence of velocity profiles a sequence of lubrication flows and the uniform pressure forces the profiles to be linear. A mass balance applied between a point just upstream of the nozzle lip edge and the downstream

point of complete solidification yields,

$$T = 1/2 \tag{13}$$

This is the classical solution of nearly-static flow in a slot coater and is recovered from Eq. 7 as $H \to 0$ when $W = 0$ corresponding to a finite lip length W^*. Ruschak (1974) discusses the role of this special solution and uses it as the basis of a perturbation analysis of the coater.

The asymptotic limits (11) are quite restrictive and cannot be achieved by varying the process parameters only. However, by altering material properties as well as process variables a sequence of experiments corresponding to limits (11) can be achieved. For example, given a fixed solidification rate, one needs an increase in wheel-speed, viscosity, and surface tension in the relationship

$$\sigma \sim V^{*3} \gg \nu \sim V^* \to \infty \tag{14}$$

If, in contrast to the ordering (14) the surface tension is less dominant,

$$\sigma \sim V^{*2} \gg \nu \sim V^* \to \infty \tag{15}$$

then the corresponding asymptotic limits may be postulated,

$$ReCa \to 0 \tag{16a}$$

$$ReH \to 0 \tag{16b}$$

with

$$Ca = \lambda H + O(H^2) \tag{16c}$$

as

$$Ca \to 0, \quad H \to 0 \tag{16d, e}$$

and the lubrication flow in region (ii) can sustain a pressure change according to Eq. 7. Pressure drops in the other regions are as in the nearly static case. The flow emerging from under the nozzle-lip need not have a linear profile and the final ribbon thickness will deviate in general from the static limit (13), as obtained from Eq. 7 in the limits (16),

$$T = \{1 + \Delta p(1 - W^2)/6\lambda W\}/(2 - W) \tag{17}$$

This flow is a version of what Higgins and Scriven (1980) terms the "viscocapillary coating bead." For an extrusion slot-coating geometry they calculate the limiting operational conditions for various meniscus boundary conditions and Higgins (1982) studies the lubrication velocity profile as it relaxes under the shear-free meniscus where the liquid emerges from the die (nozzle lip).

Finite Solidification Rates

The distinction between coating flows and the melt-spinning process begins to appear as finite solidification velocity H is accounted for. Since H also gives the slope of the lower channel wall (solidification interface) in the nearly-rectilinear flow, an increase in H from zero makes the channel convergent. The change from a parallel geometry enhances the pressure rise due to work done on the molten metal while the decrease in substrate velocity decreases the work done. This competition is accounted for (up to quadratic terms in H) in the curly bracket, obtained by a series expansion of Eq. 7,

$$\begin{aligned} p_1 - p_2 = 6(Ca/H) & \\ \cdot \{Wx_2[T(2 - Wx_2) - 1]/[1 - Wx_2]^2 & \\ + (1 - 2T)(Hx_1) & \\ + (2 - 3T)(Hx_1)^2\} & \end{aligned} \tag{18}$$

Self-consistency requires the truncation of Eq. 7 at quadratic terms since higher-order corrections have been neglected in the governing Eqs. 5. Indeed, corrections in H to order higher than the second must include contributions from the two-dimensional nature of the flow; these contributions enter through terms neglected in the approximation (5d and 5e). Although the form of the approximation (5e) suggests that the first correction to the lubrication-approximation will be at order H^2, we note that the first non-trivial correction actually occurs at order H^3 since the solution at order one is the null solution. Hence deviations from $H = 0$ through second order given by the lubrication equations are consistent with the nearly-rectilinear flow approximation. Higher-order corrections are beyond the scope of this work.

The meniscus flow compatible with the asymptotics leading to Eq. 18 is a static bead with pressure changes due to meniscus curvature. The second-order nature of the curvature differential operator requires two boundary conditions which can be taken to be the detachment position and the position at complete solidification. However, since the point of complete solidification (puddle length) is unknown an additional condition must be applied. Two sets of boundary conditions for the meniscus are considered: i) pinned with contact angle $\alpha = \pi$ (wetting) at the lip edge, Figure 5a, or pinned at the lip edge with contact angle $\beta = 0$ (no recirculation) at the downstream end of the puddle, Figure 5b; and ii) fixed contact angle $\alpha = \pi$ (wetting) but variable position of the detachment point with fixed dynamic contact angle $\beta = \Theta$ at the moving contact line, Figure 5c. These conditions will be referred to as i) pinned/$\alpha = \pi$ and pinned/$\beta = 0$, and (ii) wetted/$\beta = \Theta$.

These boundary conditions represent a variety of realizations among the class of functional relationships between contact-angle and contact-line speed. The appropriate static and moving contact line conditions for the melt-spinning problem are not known. Choosing pinned conditions allows the connection with coating flows to be established and the wetted/$\beta = \Theta$ condition is chosen on the basis of preliminary evidence from high-speed video recordings of the contact-line regions. Our treatment here is not meant to be exhaustive. In terms of the mathematics, the pinned/$\beta = 0$ condition eliminates the singularity at the point of complete solidification (recall that $\rho_s = \rho_l$ is assumed) while for all the other conditions there is a moving contact-line with the associated singularity and with recirculation at the reattachment point. For the condition pinned/$\alpha = \pi$ the relationship between contact angle and speed of the downstream moving contact line is left unspecified to be determined as part of the solution.

The pinned/$\beta = 0$ condition leads to a convex meniscus for pressures under the meniscus which are below ambient. To

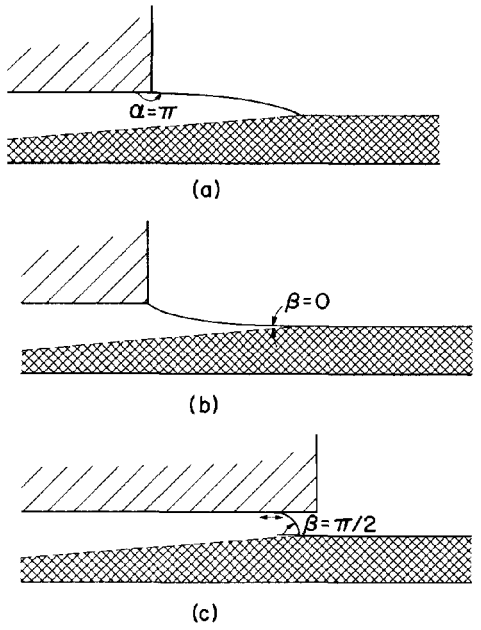

Figure 5. Contact-line conditions include: a) a pinned contact-line with wetting ($\alpha = \pi$); b) a pinned contact line with fixed downstream contact angle ($\beta = 0$); and c) a variable contact line with fixed downstream contact angle ($\beta = \theta\pi/2$).

order H^2, one obtains

$$p_2 - p_a = -(1 - T)H^2/(T - W)^2 + O(H^3) \quad (19)$$

Equation 19 combined with Eq. 18 and the uniform pressure solution to the turning flow region give the overall pressure drop,

$$\begin{aligned}\Delta p = 6\lambda\{&W[T(2 - W) - 1]/[1 - W]^2 \\ &+ (1 - 2T)(2R + n)H \\ &+ (2 - 3T)(2R + n)^2H^2\} \\ &- (1 - T)H^2/(T - W)^2 + O(H^3)\end{aligned} \quad (20)$$

Here, the integer n represents the number of gaplengths from the nozzle to the beginning of the lubrication flow measuring the extent of "entrance" effects. In summary, this implicit relationship for the ribbon thickness corresponds to a perturbation solution to order H^2 based on the limits,

$$ReCa \to 0 \quad (21a)$$

$$ReH \to 0 \quad (21b)$$

with

$$Ca = \lambda H + o(H^2) \quad (21c)$$

as

$$H \to 0 \quad (21d)$$

Equation 20 is cubic in T and of the three roots only one is physically relevant. It is plotted as a function of H in Figure 6 with the choice $n = 0$ for three different applied pressures and the other parameters as listed. Behavior near the coating flow "viscocapillary bead" limit shows thickness decreasing weakly with wheel speed for the higher applied pressures and nearly independent of wheel speed for zero applied pressure. There is a regime for zero applied pressure where thickness increases with wheel-speed, albeit weakly. Phenomenological stability arguments suggest that the portion of the curve for which thickness increases with wheel speed corresponds to an unstable solution but the full stability analysis which is necessary to confirm this and to complete the stability picture will not be taken up here. Thicknesses greater than unity correspond to meniscus pressures greater than ambient and concave meniscus shapes. These are predicted for sufficiently large applied pressures and sufficiently slow wheel speeds, neither of which are likely to be achievable due to limitations not directly included in the model. Indeed, applied pressures greater than unity will tend to blowout the upstream meniscus as previously discussed and slow wheel speed will tend to clog the nozzle (solidification front will intersect nozzle lip).

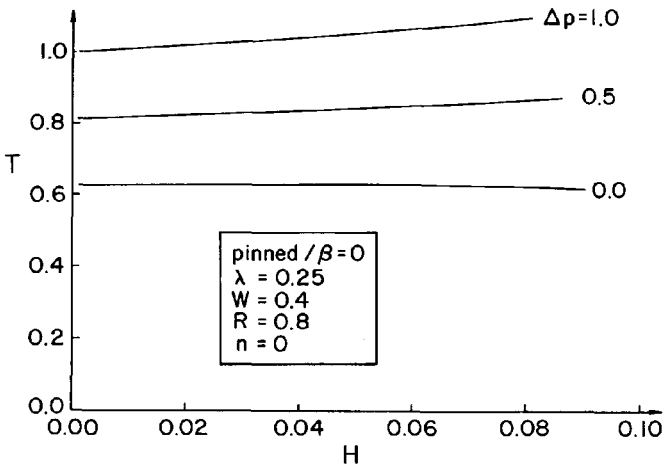

Figure 6. Ribbon thickness T v. solidification rate H with applied pressure Δp as a parameter according to Eq. 20.

The pinned/$\alpha = \pi$ condition leads to a concave meniscus which is a piece of a circle, the same piece as for pinned/$\beta = 0$ but flipped over and reflected. Therefore, the pressure drop across the meniscus is identical in magnitude but of opposite sign to Eq. 19. This leads to an overall pressure drop obtained by changing the sign of the last term in Eq. 20. Since the pressure change across the meniscus contributes at order H^2 the deviation from Eq. 20 will be small for the range of H shown in Figure 6. Indeed, a plot of thickness versus wheel-speed for these boundary conditions gives curves which are indistinguishable from those of Figure 6 over the range plotted.

The set of meniscus boundary conditions wetted/$\beta = \Theta$ yield noteworthy predictions. The solution is written

$$\begin{aligned}\Delta p = \sin\Theta/2a(1 - T) &+ (6\lambda/(1 - T))\{-T(1 - T) \\ &+ [2R + n)(1 - T)(1 - 2T) + a]H \\ &+ [(2R + n)^2(1 - T)(2 - 3T) \\ &+ 2(2R + n)a(2R + n - a - 1)]H^2\} + O(H^3)\end{aligned} \quad (22a)$$

where

$$a \equiv (1 + \cos\Theta)/\sin\Theta \qquad (22b)$$

This quadratic equation in T has two roots which may be physically reasonable for a range of applied pressures; they are plotted in Figure 7 for $\Theta = \pi/2$. In contrast to the pinned-end cases, the coating flow solutions cannot be recovered in the limit $H \rightarrow 0$. Indeed, by the model the contact line is unrestricted in its movement along the lip and consequently one of the limits of vanishing solidification rate corresponds to a contact line that moves off to infinity consistent with a ribbon thickness that approaches a limiting value of nearly the gap dimension ($T \rightarrow 1$). The other limit gives a small ribbon thickness ($T \rightarrow 0$) with large wheel-speed at an infinite puddle length. Yu's solution (Yu, 1987) can be related to this set of conditions. He assumes a pinned-end with wetting and employs the lubrication approximation both under the meniscus and within the gap region. Under these conditions the contact line at the downstream position where solidification is complete must satisfy $\beta = \pi/2$ as is known (Buckmaster, 1977). Yu obtains his solution numerically and the plot of the meniscus shape clearly shows this requirement is met. His solution therefore has a fixed contact angle at the moving contact line as well as at the static line and may be viewed as an approximation (curvatures are restricted) to one of the solutions of the family whose behavior is plotted in Figure 7. Yu's numerical data indicate that the correspondence is with the branch of solutions connected to the vanishing ribbon-thickness limit.

Figure 7 predicts no steady solution for a range of wheel speeds if the applied pressure is small enough. This behavior results from the relative contributions of the lubrication and meniscus pressure drops to the total pressure drop and is illustrated in Figure 8. Because it is concave, pressure decreases across the meniscus for all ribbon thicknesses and this pressure drop becomes infinitely large as the ribbon thickness approaches the gap dimension and the meniscus shrinks in extent. This contribution to the pressure drop is independent of H. On the other hand, the pressure change due to the lubrication flow is nonuniform in T as $H \rightarrow 0$. For $H = 0$ and because the lubrication channel length can be infinite there is a pressure rise for all thicknesses; the drag of the plate always dominates the velocity profile. However, for small H, and large mass flowrates corresponding to large thicknesses the Poiseuille pressure drop can dominate. The combined pressure drop as it depends on T can have a positive minimum if the Poiseuille contribution is sufficiently dominant. In this case an applied pressure below the minimum cannot be sustained and there is no steady solution. One might expect the meniscus to cycle between a convex and

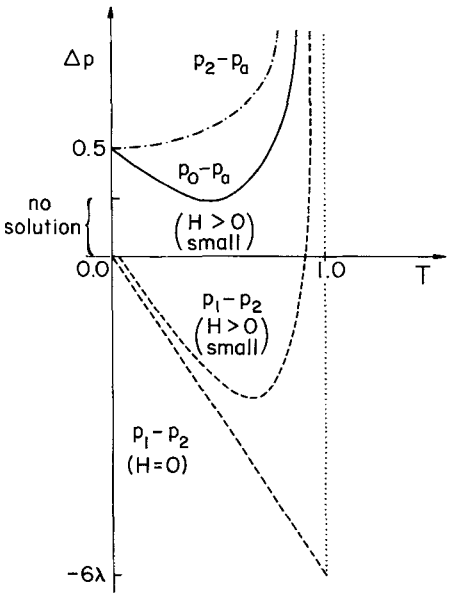

Figure 8. Overall applied pressure, $\Delta p \equiv p_0 - p_a$, is the sum of the meniscus pressure drop, $p_2 - p_a$, and the lubrication pressure change, $p_1 - p_2$, which depends on solidification rate H for the wetted/$\beta = \pi/2$ condition and varies with ribbon thickness.

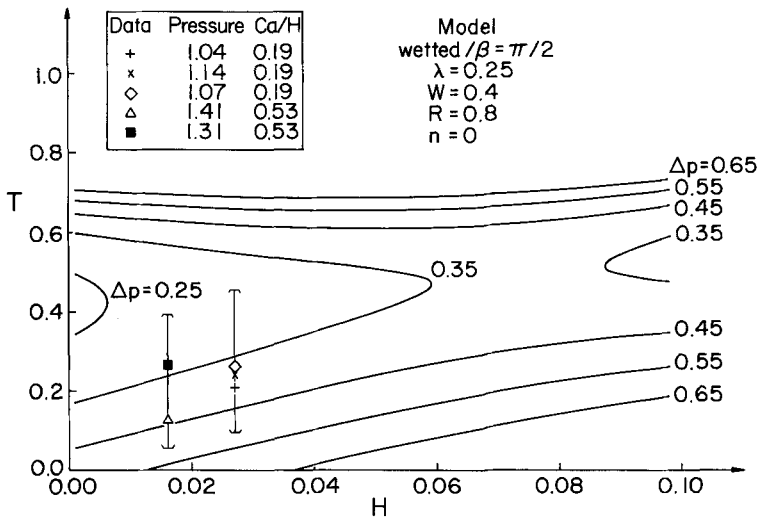

Figure 7. Ribbon thickness T v. solidification rate H with applied pressure Δp as a parameter (solid lines) according to Eq. 22 and results of experiments with error bars.

concave shape. Whatever the unsteady behavior it is certain to be a potential source for defects and irregularities in the ribbon and hence an operating regime of significant practical consequences.

Experiment

A brief discussion of the experiment illustrates some of the technical difficulties involved and serves to round out a sense of the problem. The results of experiment are reproducible, yet the experimental techniques are not developed enough to deliver data which can distinguish trends predicted by the theory. On the other hand, they present no contradictions to the theory.

The heart of the apparatus is a commercially available melt-spinner consisting of a precision-balanced copper-beryllium alloy wheel, one foot in diameter, housed in a vacuum chamber designed to enable rapid solidification in a controlled atmosphere. The wheel is connected to a variable speed drive-motor capable of producing linear velocities up to 30 m/s. A machined graphite nozzle (replaceable) is fitted to a graphite crucible and is positioned close to the wheel. An 0.08 kg charge of pure aluminum is inserted in the crucible with a stopper in place. A radio-frequency heating coil surrounds the crucible and melts the metal charge. Once the desired temperature is achieved uniformly within the melt as ascertained by a traverse of a thermocouple the stopper is released and a controlled overpressure forces the molten metal into the rapidly rotating wheel. The metal ribbon is spun off the wheel into a collecting chute.

The major source of uncertainty in the experiments is the gap separation between the nozzle and the wheel. The gap is set precisely before heating begins at a separation on the order of one millimeter. However, the thermal expansion of the graphite upon heating in the range of 1,000 K is appreciable and estimates suggest that it can reduce the gap by as much as 30–40%. The error bars on the data shown in Figure 7 are dominated by this uncertainty. Nevertheless, runs for which the initial and final gap measurements are identical yield the same ribbon thicknesses establishing reproducibility. Redesign of the apparatus to enable precise control of the "hot gap" is relatively straightforward.

Figure 7 shows data from seven runs for which a continuous ribbon was successfully formed. Three runs under identical conditions gave identical thickness and are represented by the single data symbol ◇. The measured pressures (made nondimensional) are known within ±0.5 and the experimental parameter R with uncertainty $0.4 < R < 1.2$ inherited from the uncertainty in G^* which is used to nondimensionalize R^*. The influence of applied pressure on ribbon thickness follows the trend predicted by the theory for the thin-ribbon limit in the case of the wetted/$\beta = \pi/2$ contact line condition. However, the extent of the error bars preclude a quantitative comparison.

Solutions have been developed as a perturbation of a specific asymptotic limit of well-known governing equations. It is instructive to compare the limits assumed in the theory with the values of the corresponding dimensionless parameters typical of experiment. Table 2 shows these comparisons. The typical values of H and Ca suggest that the limits $H \to 0$ and $Ca \to 0$ are reasonable while on the other hand $ReCa \to 0$ and especially $ReH \to 0$ are quite far from being satisfied. Therefore, if the theory needs to be brought more in line with the experiments some effects of inertia may need to be included. Asymptotic limits other than those in Eq. 11 or 16 might be considered or higher-order contributions to solutions obtained through limits in (11) and (16) might be included.

Table 2. Limiting Case Used in the Theory VS. Typical Values of the Dimensionless Groups for Experiment

Theory	Experiment
as $H \to 0$	$H = 0.02$
and $Ca \to 0$	$Ca = 0.005$
$Ca/H \to \lambda$	$\lambda = 0.25$
$ReCa \to 0$	$ReCa = 11.5$
$ReH \to 0$	$ReH = 46.0$

Conclusions

Evidence suggests that the heat-transfer in the planar-flow melt-spinning process can be accounted for to a first approximation by a single parameter, the solidification rate. Using this characterization we construct a framework for the fluid mechanics based on asymptotic limits of vanishing solidification rate, capillary number, and Weber number.

This framework allows the connection to a simpler and relatively well-understood class of processes to be established. If surface tension is sufficiently dominant the limiting flow is a static bead; a classical coating-flow solution is recovered. In this case the only pressure drop sustained by the system is across the meniscus. On the other hand, for strong but less dominant surface tension, a lubrication flow between the wheel and nozzle contributes a pressure change and thereby influences the final ribbon thickness. In contrast to the coating flow, the presence of the solidification front (i) makes the effective geometry of the channel dependent on a wheel-speed and (ii) allows the downstream meniscus to be concave (relative to the wheel) as well as convex.

Closed-form perturbation solutions valid to second order in solidification rate are presented for several sets of boundary conditions. These solutions are self-consistent within the specified asymptotic limits and indicate that ribbon thickness can both decrease and increase with wheel speed although it is likely that these solutions are unstable over certain portions of the parameter ranges.

Experiments undertaken show reproducible results and do not preclude agreement with theory.

Acknowledgment

The experiments were performed at the Alcoa Laboratories by J.K. Carpenter during the summer of 1987. He would like to thank Dr. Ho Yu and the Laboratories for their hospitality. P.H. Steen acknowledges partial support for this work by NSF Grant MSM 8711824 and by the U.S. Army Research Office through the Mathematical Sciences Institute of Cornell University.

Notation

dv = volume element in integration, m^3
f^* = puddle length, m
p^* = pressure, $N \cdot m^{-2}$
v^* = streamwise velocity component, $m \cdot s^{-1}$
x^* = distance from upstream contact line, m
G^* = gap between wheel and nozzle, m
H^* = solidification rate, $m \cdot s^{-1}$
R^* = nozzle half-channel dimension, m
T^* = ribbon thickness, m

V^* = linear wheel speed, $m \cdot s^{-1}$
W^* = nozzle lip length, m

Greek letters

α = contact angle at meniscus detachment, *rad*
β = contact angle at downstream contact line, *rad*
$\gamma = \langle v^{*3} \rangle / \langle v^* \rangle^3$, 1
μ = molten metal viscosity, $N \cdot s \cdot m^{-2}$
$\lambda = Ca/H$
ν = kinematic viscosity, $m^2 \cdot s^{-1}$
ρ = density, $kg \cdot m^{-3}$
σ = surface tension, $N \cdot m^{-1}$
τ = shear stress, $N \cdot m^{-2}$
Θ = specified value of downstream contact angle, *rad*
Φ^* = viscous dissipation per unit volume, $kg \cdot s^{-3} \cdot m^{-2}$
Ω = flow domain for turning region

Dimensionless parameters/groups

$a = (1 + \cos\Theta)/\sin\Theta$
$f = f^*/G^*$
$g = \langle x_1^* \rangle_{ED} V^* x_1^* / 2\sigma \langle v^* \rangle_{CD}$
$h = \int_\Omega \Phi^* dv / 2\sigma \langle v^* \rangle_{CD}$
k_g = constant in expansion of g
k_h = constant in expansion of h
$n = (x_1^* - 2R^*)/G^*$
$p = p^* G^*/2\sigma$
$\Delta p = p_o - p_a$
u = velocity in direction of x coordinate
v = velocity in direction of y coordinate
u_n = velocity component normal to interface
u_t = velocity component tangential to interface
$x_1 = x_1^*/G^*$
$x_2 = x_2^*/W^*$
A = radius of circular arc
$H = H^*/V^*$
$R = R^*/G^*$
$T = T^*/G^*$
$W = HW^*/G^*$
$Ca = \mu V^*/2\sigma$

$Re = \rho_l T^* V^*/\mu$

Subscripts

a = ambient
c = critical
l = liquid
s = solid
x = partial derivative with respect to x coordinate
y = partial derivative with respect to y coordinate
AB = cross-section at location 0
CD = cross-section at location 1
ED = section of boundary of Ω adjacent to wheel
0 = streamwise location: entrance to region i
1 = streamwise location: entrance to region ii
2 = streamwise location: entrance to region iii

Operators and symbols

$\langle \cdot \rangle$ = average over a section
$\partial/\partial n$ = partial derivative in direction normal to interface
$o(\cdot)$ = order symbol
$O(\cdot)$ = order symbol

Literature Cited

Belden, R. H., "Commercializing a New Product," *Chem. Eng. Prog.* 27 (May, 1985).

Buckmaster, J., "Viscous Sheets Advancing over Dry Beds," *J. Fluid Mech.*, **81,** 735 (1977).

Chu, M. G., A. Giron, and D. A. Granger, "Microstructure and Heat Flow in Melt-Spun Aluminum Alloys," *Proc. Int. Conf. on Rapidly Solidified Materials,* ASM, 311 (1986).

Davies, H. A., "Solidification Mechanisms in Amorphous and Crystalline Ribbon Casting," *Proc Int. Conf. on Rapidly Quenched Metals,* S. Steeb and H. Warlimont, eds., 101 (1985).

Dussan V, E. B., "On the Spreading of Liquids on Solid Surfaces: Static and Dynamic Contact Lines," *Ann. Rev. Fluid Mech.*, **11,** 371 (1979).

Guntherodt, H.-J., "Introduction to Rapidly Solidified Materials," *Proc. Int. Conf. on Rapidly Quenched Metals,* S. Steeb and H. Warlimont, eds., 1591 (1985).

Gutierrez, E. M., "The Mathematical Modelling of Metals Processing," Ph.D. Diss. Mass. Inst. of Technol. Cambridge, MA (1985).

Hanks, R. W., and H. C. Rao, "Laminar-Turbulent Transition in Ducts of Rectangular Cross Section," *Ind. Eng. Chem. Fund.*, **5,** 558 (1966).

Higgins, B. G., and L. E. Scriven, "Capillary Pressure and Viscous Pressure Drop Set Bounds on Coating Bead Operability," *Chem. Eng. Sci.*, **35,** 673 (1980).

Higgins, B. G., "Downstream Development of Two-Dimensional Visco-capillary Film Flow," *Ind. Eng. Chem. Fund.*, **21,** 168 (1982).

Hillmann, H., and H. R. Hilzinger, "On the Formation of Amorphous Ribbons by the Melt-Spin Technique," *Rapidly Quenched Metals III,* Metals Society, London (1978).

Jones, H., *Rapid Solidification of Metals and Alloys,* Instn. of Metallurgists, London (1982).

Kavesh, S., "Principles of Fabrication," *Metallic Glasses,* Amer. Soc. of Metallurgists, Metals Park, OH, 36 (1978).

Koon, N. C., "Impact of Rapid Solidification Technology on Magnetic Alloy Design," *Conf. on Rapid Solidification Processing: Principles and Technologies,* paper II.6 (1986).

Miller, J. A., "Alloying Approaches for High Strength/Oxidation Resistant Nickel-Base Superalloys Utilizing Rapid Solidification," *Conf. on Rapid Solidification Processing: Principles and Technologies,* paper II.5 (1986).

Miyazawa, K., and J. Szekely, "A Mathematical Model of the Splat Cooling Process Using the Piston and Anvil Technique," *Met. Trans. B,* **10B,** 349 (1979).

Miyazawa, K., and J. Szekely, "A Mathematical Model of the Splat Cooling Process Using the Twin-Roll Technique," *Met. Trans. A,* **12A,** 1047 (1981).

Narasimhan, D., "Continuous Casting Method for Metallic Strips," U.S. Pat. 4,142,571 (1979).

Orszag, S., "Accurate Solution of the Orr-Sommerfeld Stability Equation," *J. Fluid Mech.*, **50,** 689 (1971).

Ruschak, K. J., "The Fluid Mechanics of Coating Flows," Ph.D. Diss., Univ. of Minnesota, Minneapolis (1974).

Ruschak, K. J., "Coating Flows," *Ann. Rev. Fluid Mech.*, **17,** 65 (1985).

Yu, H., "A Fluid Mechanics Model of the Planar Flow Melt Spinning Process under Low Reynolds Number Conditions," *Met. Trans. B,* **18B,** 557 (1987).

Manuscript received Feb. 4, 1988, and revision received May 19, 1988.